

Generating GHZ states with squeezing and post-selection

Byron Alexander,^{1,*} Hermann Uys,^{1,2,†} and John J. Bollinger^{3,‡}

¹*Department of Physics,*

Stellenbosch University, Stellenbosch Central 7600, Stellenbosch, South Africa

²*Council for Scientific and Industrial Research,*

National Laser Centre, Brummeria, Pretoria, 0184, South Africa

³*National Institute of Standards and Technology, Boulder, Colorado, USA*

(Dated: December 2, 2019)

Many quantum state preparation methods rely on a combination of dissipative quantum state initialization, followed by unitary evolution to a desired target state. Here we demonstrate the usefulness of quantum measurement as an additional tool for quantum state preparation. Starting from a pure separable multipartite state, a control sequence, which includes rotation, spin squeezing via one-axis twisting, quantum measurement and post-selection, generates a highly entangled multipartite state, which we refer to as *Projected Squeezed* states (or *PS* states). Through an optimization method, we then identify parameters required to maximize the overlap fidelity of the *PS* states with the maximally entangled Greenberger-Horne-Zeilinger states (or *GHZ* states). The method leads to an appreciable decrease in state preparation time of *GHZ* states when compared to preparation through unitary evolution with one-axis twisting only.

I. INTRODUCTION

Emergent technologies, such as quantum computing, quantum communication, and quantum sensing, rely principally on quantum phenomena such as superposition and entanglement for their unique capabilities. These phenomena allow quantum computational devices to overcome limits set by their classical counterparts in computational speed of complex algorithms. Furthermore, quantum sensors [1], devices which utilize quantum correlations to improve sensitivity of measurement by suppressing phase noise in multiparticle interferometry [2–4], demonstrate the potential of quantum-enhanced technology. Examples include enhanced performance in atomic clocks [5, 6], magnetic field detection [7] and precision of frequency measurements [8, 9].

To this end, it becomes paramount to develop well-defined and efficient protocols to produce and further exercise control over states of quantum bits that exhibit desired quantum mechanical traits. Our investigation focuses on establishing a protocol that uses quantum control operations combined with measurement and post-selection to produce highly entangled metrologically relevant states. We will refer to these states as *Projected Squeezed* states (see [10–13] for relevant discussions on measures of multipartite entanglement). We further study optimization of the control parameters that produce maximal overlap of the projected squeezed state with the well-known *Greenberger-Horne-Zeilinger* state (commonly referred to as the maximally entangled state or *GHZ* state, see [10, 14]). For a multipartite system

consisting of N -qubits, the *GHZ* state reads as follows

$$|GHZ\rangle := \frac{|0\rangle^{\otimes N} + |1\rangle^{\otimes N}}{\sqrt{2}}. \quad (1)$$

Due to their high level of entanglement, the *GHZ* states are of importance in various applications such as metrology [11], quantum teleportation [15], quantum computing [16] and quantum secret sharing [17]. There are numerous proposed schemes for producing *GHZ*-states particularly in the context of cavity quantum electrodynamics [18–23]. Some of the most successful implementations have been in trapped-ion systems, where 14-ion *GHZ* states [24] and more complex entangled states of up to 20 ions [25] have been observed. Recently 20-qubit *GHZ* states have been generated through unitary evolution with Rydberg atom qubits [26] and superconducting circuit qubits [27]. Using post-selection in a linear optical system, *GHZ* states of 10 photons have been reported [28]. Closely related to the photon *GHZ* states are the so-called *NOON* states, which also exhibit an improvement on the standard quantum limit with regard to phase error measurements [29]. A number of proposed schemes for producing *NOON* states exist [30–33].

Our approach expands the typical suite of quantum state preparation tools, which relies on dissipative state initialization followed by unitary evolution, to include quantum measurement. The particular example illustrates that non-trivial speed-up can be achieved as compared to state preparation with unitary evolution only. This aspect may be of interest to beat decoherence timescales in appropriate scenarios. Measurement-based state preparation has been discussed and demonstrated for spin-squeezed states ([34, 35]). Only limited investigations have been carried out for more general state preparation protocols (for examples see [36, 37]).

The setup we have in mind is an ensemble of two-level systems, with eigenstates represented in the collective pseudo-spin basis (also known as the *Dicke state basis*

* alxbyr001@myuct.ac.za

† hermann.uys@gmail.com

‡ john.bollinger@nist.gov

[38]). The projected squeezed state is produced through a sequence of control operations including initialization, rotation, spin squeezing [39], quantum measurement and post-selection. Experimentally, the main technical challenge is carrying out a projective measurement of the collective spin projection quantum number (as opposed to a measurement in the single particle basis), as all other aspects are well established.

The one-axis twisting spin-squeezing operator (also known as the *Kitagawa Shearing Gate*), which was introduced in a seminal paper [39], is described by the following unitary transformation

$$\hat{U}_{Sq}(t) = \exp(-i\chi t \hat{J}_z^2). \quad (2)$$

One-axis twisting has been realized with trapped ions [40], neutral atoms [41, 42] and superconducting circuits [27]. Here χ quantifies the strength of the squeezing interaction, and

$$\hat{J}_k := \sum_i^N \frac{1}{2} \sigma_i^k, \quad (3)$$

where $k = x, y, z$ and σ_i^k is the k -component of the usual Pauli spin operator for the i 'th two-level system in an ensemble of N systems. This definition preserves the spin commutation relation $[\hat{J}_x, \hat{J}_y] = 2i\epsilon_{xyz}\hat{J}_z$ for the pseudo-spin $\hat{J}^2 = \hat{J}_x^2 + \hat{J}_y^2 + \hat{J}_z^2$. In what follows, we will restrict ourselves to a subspace of the full pseudo-spin Hilbert space, namely the fully symmetric (Dicke) eigenstates for which:

$$\hat{J}_z \left| \frac{N}{2}, \frac{N}{2} - m \right\rangle = \left(\frac{N}{2} - m \right) \left| \frac{N}{2}, \frac{N}{2} - m \right\rangle,$$

with $m = 0, 1, 2, \dots, N$ and

$$\hat{J}_z^2 \left| \frac{N}{2}, \frac{N}{2} - m \right\rangle = \left(\frac{N}{2} \right) \left(\frac{N}{2} + 1 \right) \left| \frac{N}{2}, \frac{N}{2} - m \right\rangle.$$

A method for constructing the Dicke states from the single spin basis is discussed in [40].

II. METHOD

We now describe the steps in the state preparation protocol. As an initial state we choose the pure, separable state

$$|\psi(0)\rangle = \left| \frac{N}{2}, \frac{N}{2} \right\rangle. \quad (4)$$

The protocol, in sequence, consists of the following operations:

Step 1 - An initial rotation by $\frac{\pi}{2}$ about the x -axis to form what is known as the *coherent spin* state (or *CS*

state)

$$|CS\rangle = \frac{1}{2^{N/2}} \sum_{M=-\frac{N}{2}}^{\frac{N}{2}} \binom{N}{\frac{N}{2} + M}^{1/2} \left| \frac{N}{2}, M \right\rangle. \quad (5)$$

We can visually represent any state, $|\psi\rangle$, on the Bloch-sphere by considering the modulus squared of the projection of that state onto a rotated coherent spin state, $H = |\langle \psi | \exp(-i\phi \hat{J}_z) \exp(-i\theta \hat{J}_x) |CS\rangle|^2$, where θ and ϕ are respectively the polar and azimuthal angles. These are commonly referred to as *Husimi plots* [43]. This projection, when $|\psi\rangle = |CS\rangle$, is shown on a unit sphere in Fig. 1(a). It shows that the rms width of H is uniform in all directions for this case.

Step 2 - The coherent spin state then undergoes *squeezing* by the unitary transformation Eq. (2), where the magnitude of squeezing is controlled by choices of the squeezing parameter χt [40]. This is shown in Fig. 1(b)-(c) for different values of χt . As we can see, when acting on a coherent spin state, the squeezing operator reduces the spin uncertainty along one spin axis at the expense of increasing the uncertainty along an orthogonal spin axis. The reduction in uncertainty occurs symmetrically about an axis tilted slightly with respect to the x -axis as opposed to the x -axis itself. A choice of the squeezing parameter of approximately $\chi t = 0.25$ starts producing a projection sufficiently flat so as to create a probability ring that wraps around the sphere (as shown in Fig. 1(c)).

Step 3 - Following the squeezing, we rotate about the x -axis until the ring is aligned with the z -axis as shown in Fig. 2.

Step 4 - The appropriate quantum measurement is carried out, and the desired state is post-selected based on the measurement outcome. The Kraus operators that describe our quantum measurement are chosen as follows:

$$A_C := \sum_M \sqrt{\Pr(M|C)} \left| \frac{N}{2}, M \right\rangle \left\langle \frac{N}{2}, M \right|, \quad (6)$$

with *Gaussian probability distribution*

$$\Pr(M|C) := \frac{1}{\sqrt{2\pi\sigma^2}} \exp\left(-\frac{(M-C)^2}{2\sigma^2}\right). \quad (7)$$

As required, the operators A_C obey the normalization condition $\int A_C A_C^\dagger dC = I$. Physically, a measurement of $A_{C'}$, with outcome C' , will project an initial wave function onto a superposition of states with amplitudes following a Gaussian distribution and centered on C' , with width σ .

Since the set of allowed measurement outcomes $\{C\}_{C \in \mathbb{R}}$ is continuous, the resultant quantum state after measurement is thus given by

$$\rho \mapsto \tilde{\rho}_{\text{final}} = \frac{A_C \rho A_C^\dagger dC}{\text{Tr}[A_C \rho A_C^\dagger dC]}, \quad (8)$$

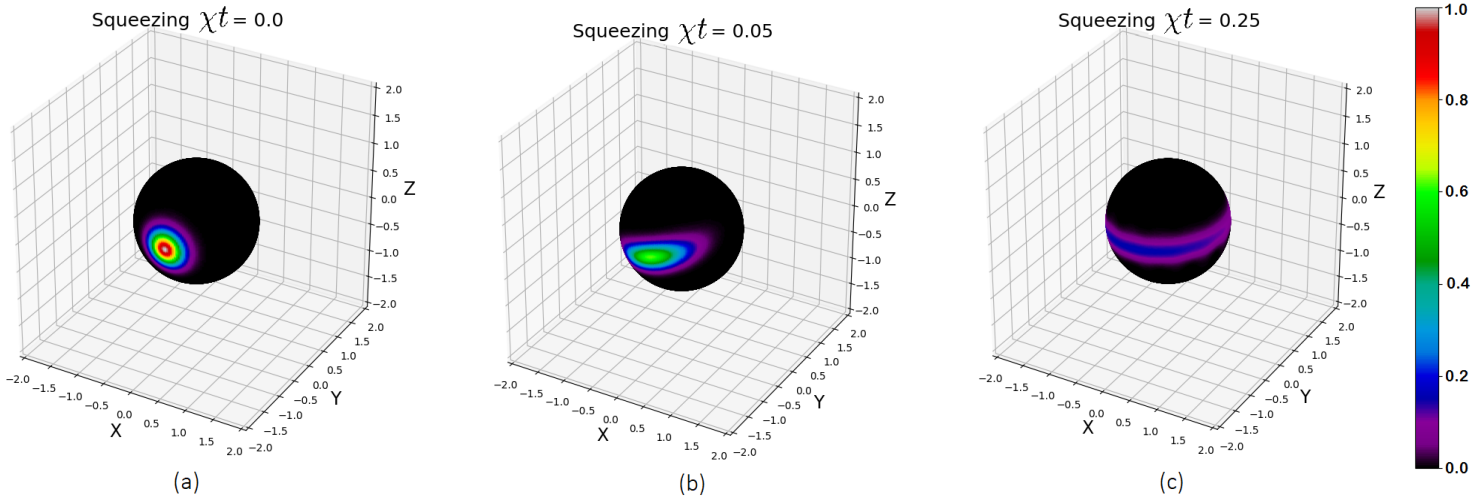


FIG. 1. Overlap fidelity of squeezed state with rotated CS state projected onto a sphere; for varied squeezing ($N = 50$).

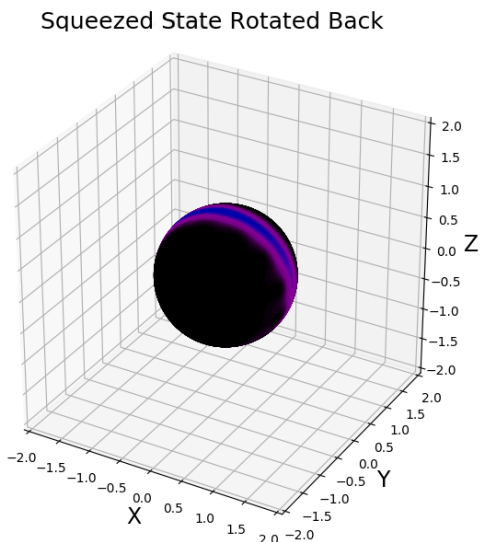


FIG. 2. Overlap fidelity with rotated CS state, after rotation, squeezing ($\chi t = 0.25$) and rotation back.

where ρ denotes the density matrix that describes the state of our system, and $\text{Tr}[A_C \rho A_C^\dagger dC]$ the probability density to observe a measurement outcome in the interval $[C, C + dC]$ (see [44]). For computational purposes we have to discretize the distribution $\text{Pr}(M|C)$ by binning the C -axis and integrating over each bin to obtain probabilities instead of probability densities, thus allowing us to model the measurement statistics numerically.

To generate the desired state, the quantum measurement defined by Eq. (6) is executed, and only outcomes with $C \approx 0$ are post-selected. This produces what we refer to as a *projected squeezed state*, henceforth denoted $|PS\rangle$. The resultant state after measurement, as shown

in Fig. 3, consists of two probability lobes concentrated on opposing sides of the Bloch-sphere. Here we used $N = 50$, $\chi t = 0.4$ and measurement operator variance $\sigma^2 = 22$ for optimization reasons which will be discussed shortly.

Step 5 - Finally, we generate a state which closely resembles the GHZ state by executing a rotation by $\frac{\pi}{2}$ about the y -axis. Then, the resemblance to the GHZ state is quantified by computing the measure of ‘closeness’ of two pure quantum states: $\mathcal{F} = |\langle PS|GHZ\rangle|^2$. \mathcal{F} is known as the *overlap fidelity*.

For completeness, we plot in Fig. 4, the modulus squared of the probability distribution of the PS state in the Dicke basis as generated in step 4 of the protocol, and after the rotation about the y -axis in step 5. It shows that any imperfect overlap is due to the unintended occupation of close-lying states other than $|\frac{N}{2}, \pm \frac{N}{2}\rangle$ with small probability amplitudes.

III. OPTIMIZATION

A numerical optimization method (random walk MCMC - Markov chain Monte Carlo type regime, see [45, 46]) is now employed to find parameters of σ^2 and χt that maximize the overlap fidelity with the GHZ state.

Given initial values of σ^2 (the variance used in defining the measurement operators) and χt (the squeezing parameter), we define an initial vector $(\sigma_0^2, \chi t_0)$. The numerical algorithm stochastically traverses the parameter space in steps defined by the vector

$$(\sigma_{step_1}^2, \chi t_{step_1}) := (\sigma_0^2, \chi t_0) + (d\sigma^2, d\chi t).$$

The increments $d\sigma^2$ and $d\chi t$ are random variables in that they are respectively chosen from Gaussian probability distributions centered at zero (with the variance of these

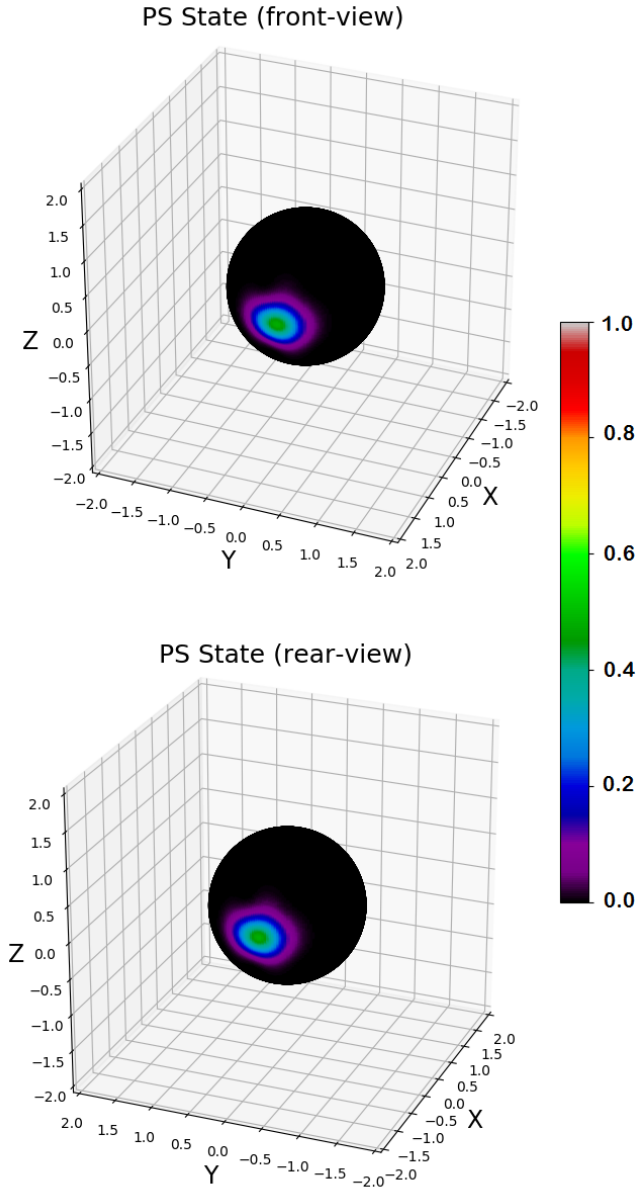


FIG. 3. Overlap fidelity of *PS* state and rotated *CS* state ($N=50$).

Gaussian distributions appropriately chosen to minimize the time of computation). For step n , the overlap fidelity is computed for parameter values $(\sigma_{step_n}^2, \chi t_{step_n})$. If the fidelity is increased, the new vector is retained, otherwise we reject the step and retain the previous vector $(\sigma_{step_{n-1}}^2, \chi t_{step_{n-1}})$. Subsequently, we compute a new step and again compare this step to the previous step. This process is continued until we identify parameters which produce an overlap fidelity value greater than or equal to a fixed threshold value. With $N = 50$, this optimization leads to maximum of $\mathcal{F} = 0.97$ for the parameters $\chi t \approx 0.4$ and $\sigma^2 = 22$.

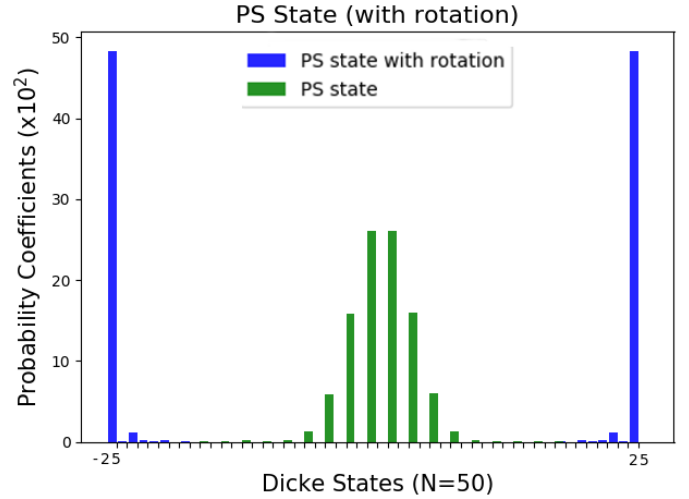


FIG. 4. Probability coefficients of *PS* state in Dicke State basis.

IV. ANALYSIS AND EFFICIENCY

To map out cross-sections of the optimization landscape, we fixed individual parameters (after they have been optimized) while allowing the others to vary. This firstly shows that the maximum fidelity monotonically increases with increasing particle number N , as illustrated in Fig. 5, for different values of χt .

In Fig. 6, χt is fixed at 0.4, and the fidelity is plotted as a function of σ^2 for different particle numbers. It confirms that the maximum fidelity increases with N , and shows that at larger particle number, the protocol is much less sensitive to variations in σ , producing high fidelity over wider regions of the variance. Figure 7 shows

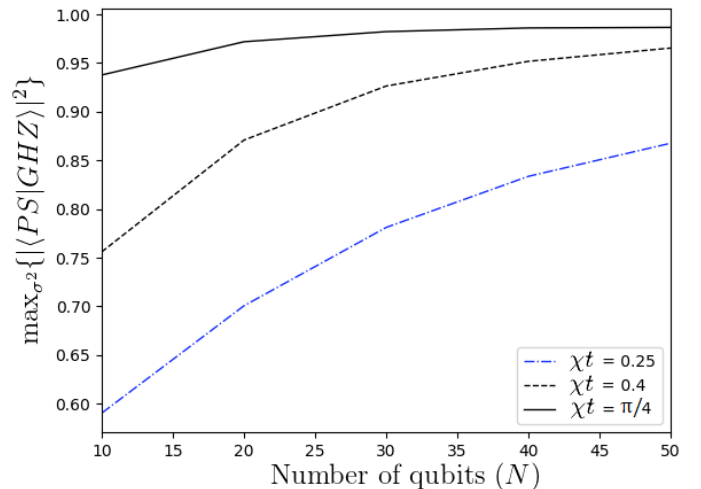


FIG. 5. Maximal *GHZ* overlap fidelity for varied squeezing times.

the fidelity as a function of variance for fixed $N = 50$, and for different values of the squeezing χt . Around $\sigma^2 = 10$, there are local maxima in \mathcal{F} at squeezing $\chi t \approx 0.25, 0.4$ and $\pi/4$.

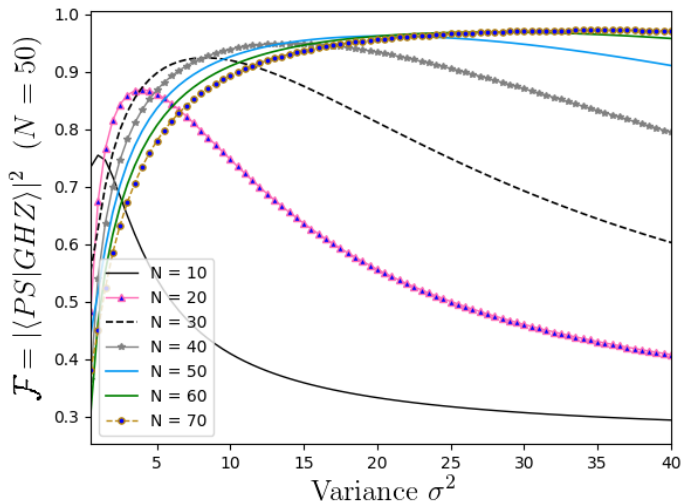


FIG. 6. Overlap fidelity of PS and GHZ states as a function of σ^2 ; for varied N ($\chi t = 0.4$).

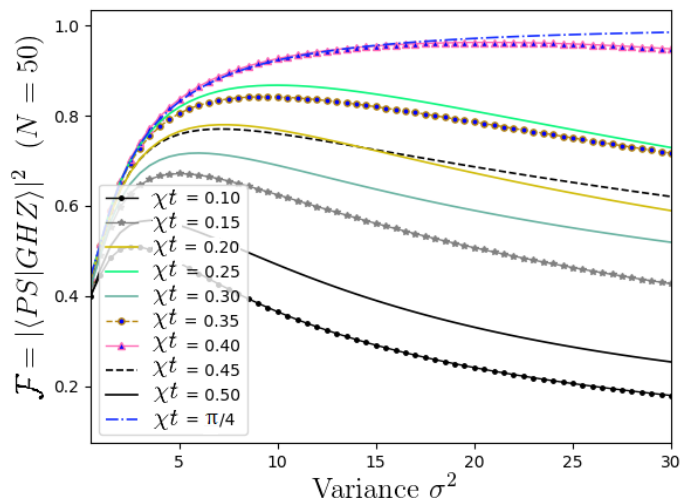


FIG. 7. Overlap fidelity of PS and GHZ states as a function of σ^2 ; for varied squeezing times ($N = 50$).

It is important to note that an exact GHZ state can be produced (with $\mathcal{F} = 1$) by using only the squeezing interaction with $\chi t = \frac{\pi}{2}$ and a rotation¹. We emphasize that

¹ In principle the PS state protocol could be employed to produce

given $\chi t \approx 0.25$ (or 0.4), our measurement-based protocol produces highly entangled GHZ type states about a factor 6 (or respectively a factor 4) faster than the coherent protocol with $\chi t = \frac{\pi}{2}$. As such, this measurement-based protocol may be preferable if a relevant decoherence timescale is close to $\chi t = \frac{\pi}{2}$.

Over and above high overlap fidelity an important consideration is the efficiency with which the PS state is produced. We will characterize a state preparation protocol as *efficient* if it requires low squeezing parameter χt (hence less time required for squeezing), produces high overlap fidelity GHZ and, given the inherent stochastic nature of the process, has a high measurement outcome probability.

Using the MCMC optimization protocol, we find that maxima in the overlap fidelity between the PS and GHZ states (varying N and σ^2) occur about squeezing parameters $\approx 0.25, 0.4$ and $\frac{\pi}{4}$ ($\chi t = \frac{\pi}{2}$ as stated above, requires no measurement). We plot in Fig. 8 the probability of obtaining measurement outcomes $\{C\}_{C \in [-60, 60]}$ for the aforementioned squeezing times. For comparison, the full pre-measurement Husimi plots are shown in Figs. 2, 9 and 10, respectively.

There are distinct probability peaks in each of the probability distributions represented in Fig. 8. These peaks are due to the probability lobes seen in the Husimi plots of the rotated squeezed state. The maxima of the central peaks correspond to our desired post-selected outcome $C' = 0$. Fig. 11 plots the overlap fidelity \mathcal{F} for each of the local maxima squeezing parameters and highlights the resultant fidelity (for select measurement outcome intervals). It shows that for $\chi t \approx 0.4$, measurement outcomes in the range $[-5, 5]$ have overlap fidelities in the range $[0.80, 0.97]$. The probability of obtaining a measurement result in this range is 0.16 (approximately 1 success for every 6 trials). There is therefore a very reasonable success ratio for projecting on states with at least moderately high overlap with the GHZ state.

Squeezing parameters $\chi t \approx 0.25, 0.4$ and $\pi/4$ respectively yield maximal PS and GHZ state fidelity values, given $C' = 0$, of 0.87, 0.97 and 0.99. A salient feature of squeezing $\chi t \approx \pi/4$, as compared to $\chi t \approx 0.25$ or 0.4 , is that the desired post-selected measurement outcome $C' = 0$ is the most probable outcome (see Fig. 8).

A. Efficiency Results

In Table I we summarize the efficiency of the protocol by showing the range (codomain) of \mathcal{F} for particular measurement outcome intervals. The analysis gives the

a state with $\mathcal{F} \rightarrow 1$ as $\sigma^2 \rightarrow \infty$ (for $\chi t = \frac{\pi}{2}$). This is clear since as the variance $\sigma^2 \rightarrow \infty$, the Gaussian distribution (7), which defines our Kraus measurement operators, tends to a uniform probability distribution and therefore the measurement operator, for $C' = 0$, approaches the identity.

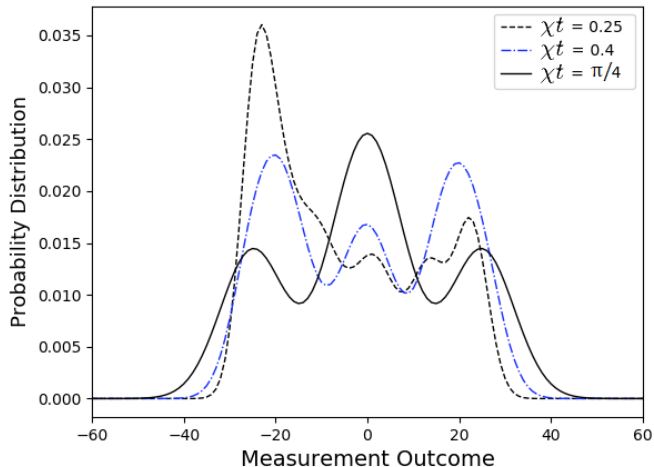


FIG. 8. Probability distribution of measurement outcomes for varied squeezing times ($N = 50$).

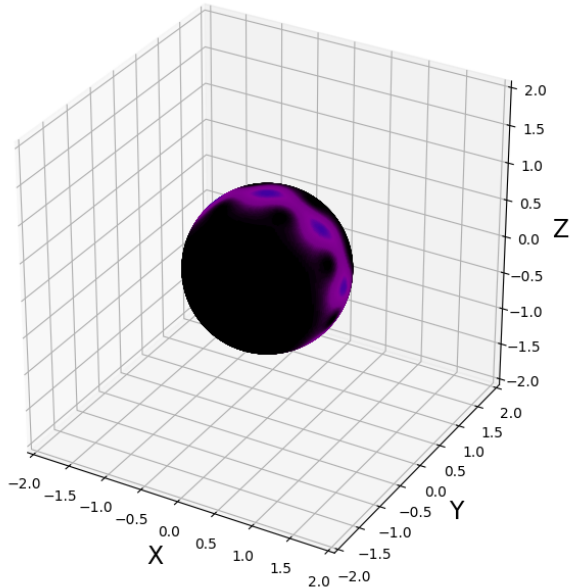


FIG. 9. Pre-measurement squeezed state ($\chi t \approx 0.4$) rotated back about x -axis.

resultant efficiency of the protocol given the optimized set of squeezing parameters (with σ^2 chosen accordingly).

V. DISCUSSION

Using the method presented one can create GHZ states with high fidelity in quantum spin systems. In trapped ion and neutral atom systems, state detection conventionally relies on fluorescence scattering from a dipole-allowed closed-cycle transition. This, however,

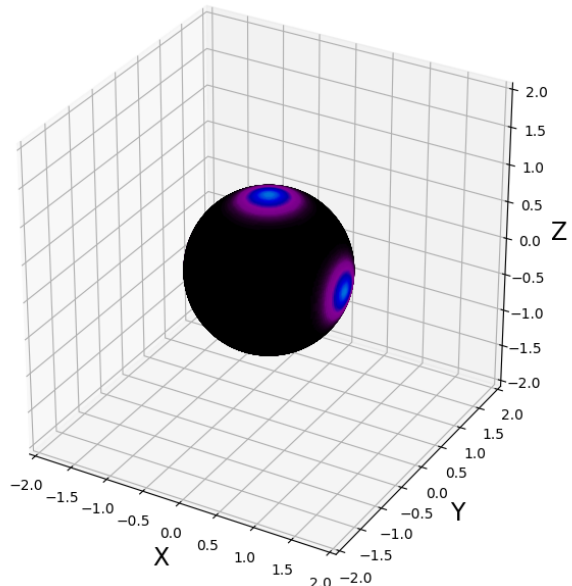


FIG. 10. Pre-measurement squeezed state ($\chi t \approx \pi/4$) rotated back about x -axis.

projects the spins in the single-particle basis rather than the Dicke basis, which makes it an unsuitable quantum measurement for our purposes. In trapped-ion systems, one potential method for executing the collective measurement is to do state dependent excitation of the ion motion using the optical dipole force [3]. The image current induced in the ion trap electrodes is expected to be proportional to the projection quantum number M and not to the individual ion state. This can be used to implement the measurement operator in Eq. (6).

Starting with the pure separable state $|\psi\rangle = |\frac{N}{2}, \frac{N}{2}\rangle$, we showed that using a combination of spin squeezing, quantum measurement and post-selection it is possible to generate many-particle GHZ states with high fidelity ($\mathcal{F} > 0.99$ given $N = 50$). It is a comparatively efficient method in the sense that, despite its stochastic nature, we produce these highly entangled PS states for squeezing parameter χt significantly lower than that required when doing coherent squeezing (2) only. This may be beneficial for beating decoherence limitations in some experiments.

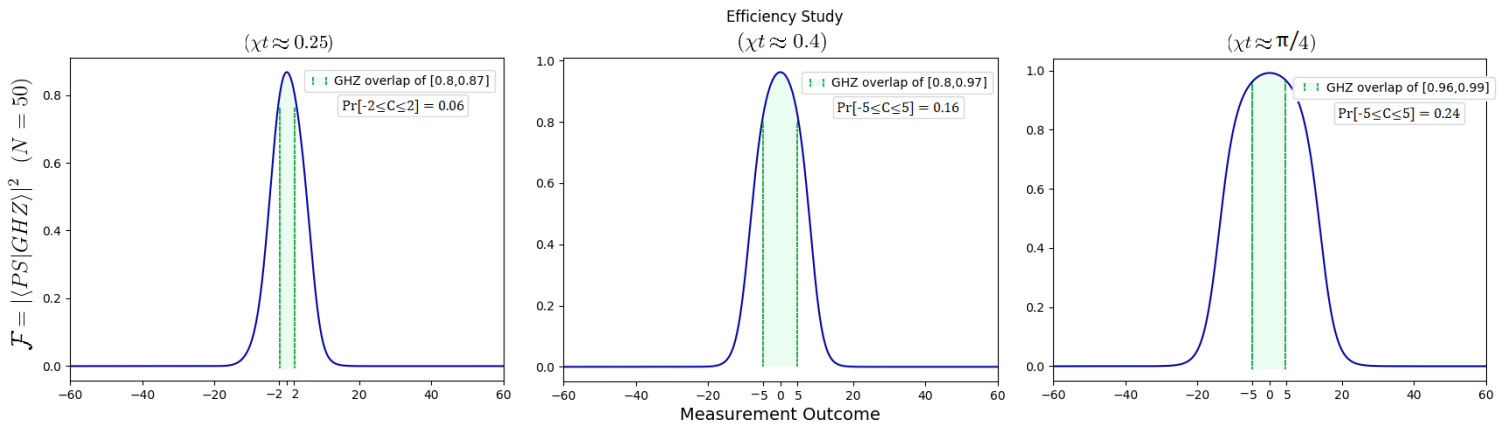


FIG. 11. Selected plots of \mathcal{F} as a function of the measured outcome C . The vertical green lines indicate the range of outcomes C that yield \mathcal{F} -values falling in the range $[\cdot, \cdot]$ indicated in the text box in each sub-figure. The total likelihood, $\Pr[\cdot]$, of observing one of those outcomes is also indicated.

$\chi t \approx 0.25$, $N = 50$, $\sigma^2 = 10.$					
$\mathcal{R}(\mathcal{F})_{C \in [-5,5]}$	$\Pr[-5 \leq C \leq 5]$	$\mathcal{R}(\mathcal{F})_{C \in [-2,2]}$	$\Pr[-2 \leq C \leq 2]$	$\mathcal{R}(\mathcal{F})_{C \in [-1,1]}$	$\Pr[-1 \leq C \leq 1]$
[0.46,0.87]	0.132	[0.80,0.87]	0.056	[0.85,0.87]	0.029
$\chi t \approx 0.4$, $N = 50$, $\sigma^2 = 22.$					
$\mathcal{R}(\mathcal{F})_{C \in [-5,5]}$	$\Pr[-5 \leq C \leq 5]$	$\mathcal{R}(\mathcal{F})_{C \in [-2,2]}$	$\Pr[-2 \leq C \leq 2]$	$\mathcal{R}(\mathcal{F})_{C \in [-1,1]}$	$\Pr[-1 \leq C \leq 1]$
[0.80,0.97]	0.161	[0.94,0.97]	0.067	[0.956,0.965]	0.035
$\chi t \approx \pi/4$, $N = 50$, $\sigma^2 = 49.$					
$\mathcal{R}(\mathcal{F})_{C \in [-10,10]}$	$\Pr[-10 \leq C \leq 10]$	$\mathcal{R}(\mathcal{F})_{C \in [-5,5]}$	$\Pr[-5 \leq C \leq 5]$	$\mathcal{R}(\mathcal{F})_{C \in [-2,2]}$	$\Pr[-2 \leq C \leq 2]$
[0.80,0.99]	0.409	[0.96,0.99]	0.242	[0.987,0.992]	0.104

TABLE I. Consider the range (co-domain) $\mathcal{R}(\cdot)$ of the overlap fidelity \mathcal{F} taken over some chosen interval $C \in [\cdot, \cdot]$ of measurement outcomes; and the respective probability $\Pr[\cdot]$ of obtaining outcomes in this interval.

VI. ACKNOWLEDGEMENTS

This project was funded by the CSIR and Department of Science and Technology. We thank E. Jordan and R.

Lewis-Swan for useful comments and discussions and I. Cirac for bringing this problem to our attention. We are also grateful to Sulona Kandhai, from the University of Cape Town, for fruitful discussions on employing numerical optimization methods.

-
- [1] C. L. Degen, F. Reinhard, and P. Cappellaro, “Quantum sensing,” *Reviews of modern physics*, vol. 89, no. 3, p. 035002, 2017.
 - [2] V. Giovannetti, S. Lloyd, and L. Maccone, “Advances in quantum metrology,” *Nature photonics*, vol. 5, no. 4, p. 222, 2011.
 - [3] O. Hosten, N. J. Engelsen, R. Krishnakumar, and M. A. Kasevich, “Measurement noise 100 times lower than the quantum-projection limit using entangled atoms,” *Nature*, vol. 529, no. 7587, p. 505, 2016.
 - [4] C. Gross, “Spin squeezing, entanglement and quantum metrology with bose-einstein condensates,” *Journal of Physics B: Atomic, Molecular and Optical Physics*, vol. 45, no. 10, p. 103001, 2012.
 - [5] E. M. Kessler, P. Komar, M. Bishof, L. Jiang, A. S. Sørensen, J. Ye, and M. D. Lukin, “Heisenberg-limited atom clocks based on entangled qubits,” *Physical review letters*, vol. 112, no. 19, p. 190403, 2014.
 - [6] P. Komar, E. M. Kessler, M. Bishof, L. Jiang, A. S. Sørensen, J. Ye, and M. D. Lukin, “A quantum network

- of clocks,” *Nature Physics*, vol. 10, no. 8, p. 582, 2014.
- [7] T. Ruster, H. Kaufmann, M. Luda, V. Kaushal, C. Schmiegelow, F. Schmidt-Kaler, and P. UG, “Entanglement-based dc magnetometry with separated ions,” *Physical Review X*, vol. 7, p. 031050, 2017.
- [8] S. F. Huelga, C. Macchiavello, T. Pellizzari, A. K. Ekert, M. B. Plenio, and J. I. Cirac, “Improvement of frequency standards with quantum entanglement,” *Physical Review Letters*, vol. 79, no. 20, p. 3865, 1997.
- [9] F. M. Ciurana, G. Colangelo, L. Slodička, R. Sewell, and M. Mitchell, “Entanglement-enhanced radio-frequency field detection and waveform sensing,” *Physical review letters*, vol. 119, no. 4, p. 043603, 2017.
- [10] M. Walter, D. Gross, and J. Eisert, “Multi-partite entanglement,” *arXiv preprint arXiv:1612.02437*, 2016.
- [11] G. Tóth and I. Apellaniz, “Quantum metrology from a quantum information science perspective,” *Journal of Physics A: Mathematical and Theoretical*, vol. 47, no. 42, p. 424006, 2014.
- [12] V. Coffman, J. Kundu, and W. K. Wootters, “Distributed entanglement,” *Physical Review A*, vol. 61, no. 5, p. 052306, 2000.
- [13] D. A. Meyer and N. R. Wallach, “Global entanglement in multiparticle systems,” *Journal of Mathematical Physics*, vol. 43, no. 9, pp. 4273–4278, 2002.
- [14] D. M. Greenberger, M. A. Horne, and A. Zeilinger, “Going beyond bells theorem,” in *Bells theorem, quantum theory and conceptions of the universe*, pp. 69–72, Springer, 1989.
- [15] V. Gorbachev and A. Trubilko, “Quantum teleportation of an einstein-podolsy-rosen pair using an entangled three-particle state,” *Journal of Experimental and Theoretical Physics*, vol. 91, no. 5, pp. 894–898, 2000.
- [16] D. Gottesman and I. L. Chuang, “Demonstrating the viability of universal quantum computation using teleportation and single-qubit operations,” *Nature*, vol. 402, no. 6760, p. 390, 1999.
- [17] M. Hillery, V. Bužek, and A. Berthiaume, “Quantum secret sharing,” *Physical Review A*, vol. 59, no. 3, p. 1829, 1999.
- [18] E. Guerra*, “Realization of ghz states and the ghz test via cavity qed,” *Journal of Modern Optics*, vol. 52, no. 9, pp. 1275–1291, 2005.
- [19] C.-L. Zhang, W.-Z. Li, and M.-F. Chen, “Generation of w state and ghz state of multiple atomic ensembles via a single atom in a nonresonant cavity,” *Optics Communications*, vol. 312, pp. 269–274, 2014.
- [20] M. Izadyari, M. Saadati-Niari, R. Khadem-Hosseini, and M. Amniat-Talab, “Creation of n-atom ghz state in atom-cavity-fiber system by multi-state adiabatic passage,” *Optical and Quantum Electronics*, vol. 48, no. 1, p. 71, 2016.
- [21] S.-B. Zheng, “One-step synthesis of multiatom greenberger-horne-zeilinger states,” *Physical review letters*, vol. 87, no. 23, p. 230404, 2001.
- [22] Z.-h. Chen, P. Pei, F.-y. Zhang, and H.-s. Song, “One-step preparation of three-particle greenberger–horne–zeilinger states in cavity quantum electrodynamics,” *JOSA B*, vol. 29, no. 7, pp. 1744–1749, 2012.
- [23] X. Zhang, Y.-H. Chen, Z.-C. Shi, W.-J. Shan, J. Song, and Y. Xia, “Generation of three-qubit greenberger–horne–zeilinger states of superconducting qubits by using dressed states,” *Quantum Information Processing*, vol. 16, no. 12, p. 309, 2017.
- [24] T. Monz, P. Schindler, J. T. Barreiro, M. Chwalla, D. Nigg, W. A. Coish, M. Harlander, W. Hänsel, M. Hennrich, and R. Blatt, “14-qubit entanglement: Creation and coherence,” *Physical Review Letters*, vol. 106, no. 13, p. 130506, 2011.
- [25] N. Friis, O. Marty, C. Maier, C. Hempel, M. Holzäpfel, P. Jurcevic, M. B. Plenio, M. Huber, C. Roos, R. Blatt, *et al.*, “Observation of entangled states of a fully controlled 20-qubit system,” *Physical Review X*, vol. 8, no. 2, p. 021012, 2018.
- [26] A. Omran, H. Levine, A. Keesling, G. Semeghini, T. T. Wang, S. Ebadi, H. Bernien, A. S. Zibrov, H. Pichler, S. Choi, *et al.*, “Generation and manipulation of schrödinger cat states in rydberg atom arrays,” *arXiv preprint arXiv:1905.05721*, 2019.
- [27] C. Song, K. Xu, H. Li, Y. Zhang, X. Zhang, W. Liu, Q. Guo, Z. Wang, W. Ren, J. Hao, *et al.*, “Observation of multi-component atomic schrödinger cat states of up to 20 qubits,” *arXiv preprint arXiv:1905.00320*, 2019.
- [28] X.-L. Wang, L.-K. Chen, W. Li, H.-L. Huang, C. Liu, C. Chen, Y.-H. Luo, Z.-E. Su, D. Wu, Z.-D. Li, *et al.*, “Experimental ten-photon entanglement,” *Physical review letters*, vol. 117, no. 21, p. 210502, 2016.
- [29] J. P. Dowling, “Quantum optical metrology—the lowdown on high-n00n states,” *Contemporary physics*, vol. 49, no. 2, pp. 125–143, 2008.
- [30] K. T. Kapale and J. P. Dowling, “Bootstrapping approach for generating maximally path-entangled photon states,” *Physical review letters*, vol. 99, no. 5, p. 053602, 2007.
- [31] M. Mitchell, “Metrology with entangled states,” in *Quantum Communications and Quantum Imaging III*, vol. 5893, p. 589310, International Society for Optics and Photonics, 2005.
- [32] P. Kok, H. Lee, and J. P. Dowling, “Creation of large-photon-number path entanglement conditioned on photodetection,” *Physical Review A*, vol. 65, no. 5, p. 052104, 2002.
- [33] G. Pryde and A. White, “Creation of maximally entangled photon-number states using optical fiber multiplexers,” *Physical Review A*, vol. 68, no. 5, p. 052315, 2003.
- [34] K. C. Cox, G. P. Greve, J. M. Weiner, and J. K. Thompson, “Deterministic squeezed states with collective measurements and feedback,” *Physical review letters*, vol. 116, no. 9, p. 093602, 2016.
- [35] M. H. Schleier-Smith, I. D. Leroux, and V. Vuletić, “States of an ensemble of two-level atoms with reduced quantum uncertainty,” *Physical review letters*, vol. 104, no. 7, p. 073604, 2010.
- [36] M. A. Nielsen, “Quantum computation by measurement and quantum memory,” *Physics Letters A*, vol. 308, no. 2–3, pp. 96–100, 2003.
- [37] Y. Yan, Z. Jian, W. Lu, X. Bao-Ming, W. Chao-Quan, and S. Bin, “Quantum state preparation and protection by measurement-based feedback control against decoherence,” *Communications in Theoretical Physics*, vol. 63, no. 2, p. 149, 2015.
- [38] R. H. Dicke, “Coherence in spontaneous radiation processes,” *Physical review*, vol. 93, no. 1, p. 99, 1954.
- [39] M. Kitagawa and M. Ueda, “Squeezed spin states,” *Physical Review A*, vol. 47, no. 6, p. 5138, 1993.
- [40] H. Uys, M. Biercuk, J. Britton, and J. J. Bollinger, “Toward spin squeezing with trapped ions,” in *AIP Confer-*

- ence Proceedings*, vol. 1469, pp. 108–121, AIP, 2012.
- [41] J. Hu, W. Chen, Z. Vendeiro, A. Urvoy, B. Braverman, and V. Vuletić, “Vacuum spin squeezing,” *Physical Review A*, vol. 96, no. 5, p. 050301, 2017.
- [42] W. Müssel, H. Strobel, D. Linnemann, D. Hume, and M. Oberthaler, “Scalable spin squeezing for quantum-enhanced magnetometry with bose-einstein condensates,” *Physical review letters*, vol. 113, no. 10, p. 103004, 2014.
- [43] C. Lee, “Q representation of the atomic coherent states and the origin of fluctuations in superfluorescence,” *Physical Review A*, vol. 30, no. 6, p. 3308, 1984.
- [44] K. Jacobs, *Quantum measurement theory and its applications*. Cambridge University Press, 2014.
- [45] W. Gilks, S. Richardson, and D. Spiegelhalter, “Markov chain monte carlo in practice, chapman & hall/crc interdisciplinary statistics,” 1995.
- [46] C. Sherlock, P. Fearnhead, G. O. Roberts, *et al.*, “The random walk metropolis: linking theory and practice through a case study,” *Statistical Science*, vol. 25, no. 2, pp. 172–190, 2010.